IEEE Access
Multidisciplinary | Rapid Review | Open Access Journal

Received January 13, 2019, accepted January 24, 2019, date of publication January 31, 2019, date of current version February 20, 2019.

Digital Object Identifier 10.1109/ACCESS.2019.2896070

In-Phase T-Junction: Study and Application to Gysel Power Dividers for High Power-Division Ratios Requiring No High-Impedance Transmission-Line Section

HEE-RAN AHN, (Senior Member, IEEE), AND MANOS M. TENTZERIS, (Fellow, IEEE)
School of Electrical and Computer Engineering, Georgia Institute of Technology, Atlanta, GA 30332, USA

Corresponding author: Hee-Ran Ahn (hranahn@gmail.com)

This work was supported by the NSF.

ABSTRACT A novel Gysel power divider, which can be fabricated without a need for any high-impedance transmission-line section (TL), even for the power-division ratios higher than 15 dB, is presented. To derive its design formulas, a new study on the conventional in-phase T-junctions is carried out, and two conditions are newly derived for the arbitrary power-division ratios and perfect matching at all the ports, which can be applied for any symmetric or asymmetric Gysel power divider without any additional effort to design the isolation circuit. As a proof-of-concept demonstration, two prototypes I and II at the design frequency of 1 GHz are fabricated for the power-division ratios of 17 and 20 dB, respectively. Such power-division ratios have never been tried before not only for the Gysel power dividers but also for generic planar power divider topologies without the use of high-impedance TLs for the wider bandwidths. The measured results are in good agreement with the predictions.

INDEX TERMS In-phase T-junctions, Gysel power dividers, high power-division ratios, ring hybrids, rat-race couplers, Wilkinson power dividers, arbitrary power-division ratios, three- and four-port power dividers.

I. INTRODUCTION

Power dividers with the in-phase T-junctions are key components in microwave circuits and have been used for various applications such as antenna feeding networks, high power amplifiers and mixers. In general, they can be classified into three-port power dividers such as Wilkinson [1]–[9] and Gysel [2], [10]–[15] power dividers, four-port power dividers like ring hybrids (rat-race couplers) [16]–[27] and multi-port power dividers. For general applications, the power dividers featuring high power-division ratios are indispensable, but their planar implementation for the power-division ratios higher than 10 dB is extremely difficult, mainly due to that the feasible range of characteristic impedances of the utilized transmission-line section (TL) is limited in microstrip format.

To overcome the problems, ''composite'' high impedance TLs consisting of TLs and series inductances which have to be realized with chip inductors [3], [7], [17], consisting of coupled TLs [8], [17] or consisting of TLs and shunt inductances/short stubs [6] and other ''composite'' TL topologies with shunt/ series inductances and capacitances [23] have been applied to those power dividers for high power-division ratios.

However, for operating frequencies higher than 5 GHz, the use of the series lumped-element inductances [3], [7], [17] can cause serious problems, due to parasitic effects, self-resonance frequencies and tolerances of the chip inductors. The applications of topologies with the coupled TLs [8], [17] are restricted due to inevitable 180° phase shifts. The method utilizing shunt inductances/ short stubs [6], [23] should typically suffer from narrow bandwidths.

Several efforts for the implementation of three-port power dividers [4], [5] and of the ring hybrids [20], [22] have been attempted without using such high-impedance TLs, but the achieved bandwidths [4], [5], [20] should be reduced proportionally to the power-division ratios, while the theory in [22] seems to be incomplete.

The associate editor coordinating the review of this manuscript and approving it for publication was Kuang Zhang.

To alleviate the conventional problems, in this paper, the in-phase T-junctions are studied, from which two conditions are newly derived for all port matching and power-division ratios. A novel topology of in-phase T-junctions for wide bandwidths and high power-division ratios is suggested, consisting of two TLs whose characteristic impedances and electrical lengths can be all different and applied to the novel Gysel power divider for high power applications without a need requiring high impedance TLs even for the extremely high power-division ratios. The design formulas for the suggested Gysel power dividers are derived based on the derived two conditions, and the frequency performances are verified with the simulated responses.

As a proof-of-concept demonstration, two prototypes I and II of Gysel power dividers for wide bandwidths are fabricated for the power-division ratios of 17 dB and 20 dB respectively, which can be regarded as the highest power-division ratio among generic planar power divider topologies ever recorded without the use of high impedance TLs. The measured responses show good agreement with the predictions.

II. IN-PHASE T-JUNCTIONS

The most important circuit of the Gysel power divider, that is terminated in equal impedances, is the in-phase T-junction. The typical in-phase T-junction is depicted in Fig. 1, where port ① terminated in an admittance Y_0 is located in the middle, and the two other ports ② and ③ are placed at both ends with no need for specific termination impedances. The characteristic admittance and the electrical length of the single TL between ports ① and ② is Y_a and Θ_a, respectively, while those of the other one located between ports ① and ③ are Y_b and Θ_b.

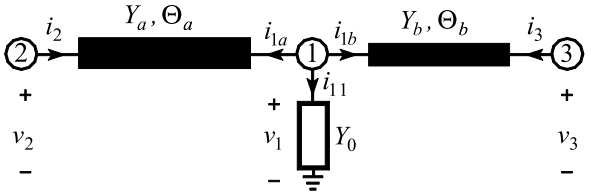

FIGURE 1. In-phase T-junction.

For the derivation of the admittance parameters in Fig. 1, the currents i_2 at port ②, i_3 at port ③ and i_{1a}, i_{1b} and i_{11} at port ① are indicated along with the corresponding voltages v_1, v_2 and v_3.

The relations between the currents and voltages of the two TLs are

$$\begin{bmatrix} i_2 \\ i_{1a} \end{bmatrix} = \begin{bmatrix} Y_{11a} & Y_{12a} \\ Y_{21a} & Y_{22a} \end{bmatrix} \begin{bmatrix} v_2 \\ v_1 \end{bmatrix} \tag{1a}$$

$$\begin{bmatrix} i_{1b} \\ i_3 \end{bmatrix} = \begin{bmatrix} Y_{11b} & Y_{12b} \\ Y_{21b} & Y_{22b} \end{bmatrix} \begin{bmatrix} v_1 \\ v_3 \end{bmatrix} \tag{1b}$$

$$i_{1a} + i_{1b} + i_{11} = i_{1a} + i_{1b} + Y_0 v_1 = 0 \tag{1c}$$

where [27]

$$\begin{bmatrix} Y_{11a} & Y_{12a} \\ Y_{21a} & Y_{22a} \end{bmatrix} = \begin{bmatrix} -jY_a\cot\Theta_a & jY_a\csc\Theta_a \\ jY_a\csc\Theta_a & -jY_a\cot\Theta_a \end{bmatrix} \tag{1d}$$

$$\begin{bmatrix} Y_{11b} & Y_{12b} \\ Y_{21b} & Y_{22b} \end{bmatrix} = \begin{bmatrix} -jY_b\cot\Theta_b & jY_b\csc\Theta_b \\ jY_b\csc\Theta_b & -jY_b\cot\Theta_b \end{bmatrix} \tag{1e}$$

Substituting i_{1a} and i_{1b} in (1a) and (1b) into (1c) gives

$$Y_{21a}v_2 + Y_{22a}v_1 + Y_{11b}v_1 + Y_{12b}v_3 + v_1Y_0 = 0 \tag{2}$$

From (2), v_1 can be derived as

$$v_1 = -\frac{Y_{21a}v_2 + Y_{12b}v_3}{Y_{11b} + Y_{22a} + Y_0} \tag{3}$$

Substituting v_1 (3) into i_2 and i_3 in (1a) and (1b) gives the relations between the currents i_2 and i_3 and the voltages v_2 and v_3 as

$$i_2 = Y_{11a}v_2 - Y_{12a}\frac{Y_{21a}v_2 + Y_{12b}v_3}{Y_{11b} + Y_{22a} + Y_0} \tag{4a}$$

$$i_3 = -Y_{21b}\frac{Y_{21a}v_2 + Y_{12b}v_3}{Y_{11b} + Y_{22a} + Y_0} + Y_{22b}v_3 \tag{4b}$$

The admittance parameters of the in-phase T-junction can be derived from (4) as

$$Y_{11} = Y_{11a} - \frac{Y_{12a}Y_{21a}}{Y_{11b} + Y_{22a} + Y_0} \tag{5a}$$

$$Y_{12} = Y_{21} = -\frac{Y_{12a}Y_{12b}}{Y_{11b} + Y_{22a} + Y_0} \tag{5b}$$

$$Y_{22} = Y_{22b} - \frac{Y_{12b}Y_{21b}}{Y_{11b} + Y_{22a} + Y_0} \tag{5c}$$

Based on the expressions in (5), the admittance parameters of the Gysel power divider in [15] for $k^2 = 9$, the conventional ring hybrids in [18] and [24] for $k^2 = 9$, 2 and 1 and another type of ring hybrids in [19] and [20] for $k^2 = 1$ and 9, respectively, are listed in Table 1 where the power-division ratio of k^2 is defined as $k^2 = (|S_{21}| / |S_{31}|)^2$ in Fig. 1. The design parameters of $Z_a^{-1} = Y_a$, Θ_a, $Z_b^{-1} = Y_b$ and Θ_b have been calculated for the equal termination impedances $Z_0 = Y_0^{-1} = 50\ \Omega$, and the admittance parameters are multiplied by 100 for easier understanding of their value range.

From the calculated values of Y_{11} and Y_{22}, one can understand that the power-division ratio of k^2 is equal to the ratio of $Re(Y_{11})$ to $Re(Y_{22})$, and the sum of $Y_{11} + Y_{22}$ should be the same as Y_0. That is, $Re(Y_{11})/Re(Y_{22})$ is the condition for the implementation of the power-division ratio of k^2, while $Y_{11} + Y_{22} = Y_0$ is that to achieve near-perfect matching at all ports. In other words, even if the in-phase T-junction in Fig. 1 is not a perfect power divider, only if these two conditions are satisfied, the "perfect" power divider properties can be obtained automatically without any additional effort to design the rest part (the balun part) [24], [25], which will be in more detail discussed and verified later.

TABLE 1. Admittance parameters of conventional in-phase T-junctions.

refs.	k^2	$Z_a^{-1} = Y_a, \Theta_a$ $Z_b^{-1} = Y_b, \Theta_b$	$\begin{bmatrix} Y_{11} & Y_{12} \\ Y_{21} & Y_{22} \end{bmatrix}$
[15]	9	$Z_a = 47.14\ \Omega$ $Z_b = 141.43\ \Omega$ $\Theta_a = \Theta_b = 60^o$	$100\ Y_{11} = 1.8 + j\ 0.24$ $100\ Y_{22} = 0.2 - j\ 0.24$
[18] [24]	9	Z_a =52.7 Ω Z_b =158.11 Ω $\Theta_a = \Theta_b = 90^o$	$100\ Y_{11} = 1.8$ $100 Y_{22} = 0.2$
	2	Z_a =61.24 Ω Z_b =86.60 Ω $\Theta_a = \Theta_b = 90^o$	$100 Y_{11} = 1.33$ $100 Y_{22} = 0.66$
	1	$Z_a = Z_b = 70.7\Omega$ $\Theta_a = \Theta_b = 90^o$	$100\ Y_{11} = 1$ $100\ Y_{22} = 1$
[19]	1	$Z_a = Z_b = 58\ \Omega$ $\Theta_a = \Theta_b = 60^o$	$100\ Y_{11} = 1$ $100\ Y_{22} = 1$
[20]	9	$Z_a = Z_b$ =50 Ω $\Theta_a = 19.17^o$ $\Theta_b = 80.14^o$	$100\ Y_{11}$ =1.8 - j0.26 $100 Y_{22} = 0.2 + j\ 0.26$

III. GYSEL POWER DIVIDERS FOR HIGH POWER-DIVISION RATIOS

Observing the relationship between the characteristic impedances of the TLs and the power-division ratios of k^2 in Table 1, one can understand that the high power-division ratios can be obtained as a result of not only a large difference between the characteristic impedances of the two TLs [15] for the in-phase T-junction in Fig. 1 but also due to the difference between two electrical lengths of the TLs in [20]. Therefore, it can be concluded that the high power-division ratios can be feasible by controlling both characteristic impedances and electrical lengths of the TLs without requiring high values of characteristic impedances.

The in-phase T-junction and its isolation circuit (*IC*) are depicted in Fig. 2 as the suggested Gysel power divider. As far as the admittance parameters of the in-phase T-junction can satisfy the two conditions derived from the Table 1, the *IC* can be easily realized accordingly without any additional effort. The power excited at port ① is divided between ports ② and ③ with the power-division ratio of k^2 where k is assumed to be $k \geq 1$.

As derived in Table 1, the two necessary conditions that enable the power-division ratios of k^2 and the perfect matching at all ports are

$$\frac{Re(Y_{11})}{Re(Y_{22})} = k^2 = \frac{|S_{21}|^2}{|S_{31}|^2} \tag{6a}$$

$$Y_{11} + Y_{22} = Y_0 \tag{6b}$$

From the derived admittance parameters in (5), the real and imaginary parts of Y_{11} and Y_{22} can be derived as

$$\mathrm{Re}\,(Y_{11}) = \frac{(Y_a \csc\Theta_a)^2\, Y_0}{T^2 + Y_0^2} \tag{7a}$$

$$\mathrm{Im}\,(Y_{11}) = -Y_a \cot\Theta_a + \frac{(Y_a \csc\Theta_a)^2\, T}{T^2 + Y_0^2} \tag{7b}$$

$$\mathrm{Re}\,(Y_{22}) = \frac{(Y_b \csc\Theta_b)^2\, Y_0}{T^2 + Y_0^2} \tag{7c}$$

$$\mathrm{Im}\,(Y_{22}) = -Y_b \cot\Theta_b + \frac{(Y_b \csc\Theta_b)^2\, T}{T^2 + Y_0^2} \tag{7d}$$

$$\text{where} \quad T = Y_a \cot\Theta_a + Y_b \cot\Theta_b \tag{7e}$$

Applying the two conditions (6) to those (7) gives the design formulas as

$$Z_a = Z_0 \sqrt{\left(\frac{k^2+1}{k^2}\right)\csc^2\Theta_a - \left(\cot\Theta_a + \frac{\cos\Theta_b}{k \sin\Theta_a}\right)^2} \tag{8a}$$

$$Z_b = Z_0 \sqrt{\left(k^2+1\right)\csc^2\Theta_b - \left(\cot\Theta_b + \frac{k\cos\Theta_a}{\sin\Theta_b}\right)^2} \tag{8b}$$

When $\Theta_a = \Theta_b$, the design formulas in (8) are identical to those in [15]. When $Z_a = Z_b = \sqrt{2}\, Z_0$ and $\Theta_b = 90°$, they are the same as those in [5]. When $Z_a = Z_b = Z_0$, they are the same as those in [20]. When $\Theta_a \neq \Theta_b$, they are the same as those in [21]. When $\Theta_a = \Theta_b = 90°$, they are the same as those in [18] and [24].

A. ISOLATION CIRCUITS

Perfect matching at ports ② and ③ and prefect isolation between ports ② and ③ in Fig. 2(a) can be achieved by connecting the in-phase T-junction and the *IC* in parallel as shown in Fig. 2, leading to following relationship.

$$\begin{bmatrix} Y_{11} & Y_{12} \\ Y_{21} & Y_{22} \end{bmatrix} + \begin{bmatrix} Y_{11\_IC} & Y_{12\_IC} \\ Y_{21\_IC} & Y_{22\_IC} \end{bmatrix} = Y_0 \begin{bmatrix} 1 & 0 \\ 0 & 1 \end{bmatrix} \tag{9}$$

where Y_{11}, Y_{12} and Y_{22} are the admittance parameters of the in-phase T-junction in Fig. 2(a), while Y_{11_IC}, $Y_{12\_IC} = Y_{21\_IC}$ and Y_{22_IC} are those of the *IC*. Substituting (6b) into (9), the admittance parameters of the *IC* can be obtained as

$$\begin{bmatrix} Y_{11\_IC} & Y_{12\_IC} \\ Y_{21\_IC} & Y_{22\_IC} \end{bmatrix} = \begin{bmatrix} Y_{22} & -Y_{12} \\ -Y_{21} & Y_{11} \end{bmatrix} \tag{10}$$

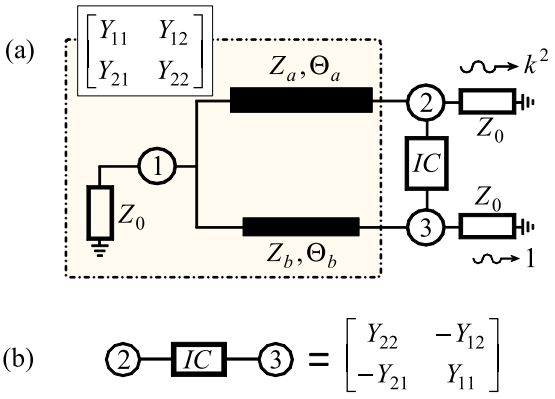

FIGURE 2. Proposed Gysel power divider. (a) Gysel power divider. (b) IC.

Comparing both admittance parameters of in-phase T-junction in Fig. 2(a) and *IC* in (10), it can be easily observed

that both Y_{11} and Y_{22} are interchanged and a negative sign is added to Y_{12} of the *IC*. That is, the *IC* topology should be effectively similar to the in-phase T-junction interchanging the ports positions ("turned around" topology), and the phase difference between the two should be 180°, referring to $-Y_{12}$. There exist numerous ways of realizing the *IC* featuring (10); three of them are shown in Fig. 3 where the in-phase T-junction is turned around, and an additional 180° TL with an arbitrary value of the characteristic impedance Z_i is inserted between the TL with Z_b and the resistor of R_0 or between the TL with Z_a and R_0 as shown in Fig. 3(a) and (b), respectively. In this case, the value of R_0 should be the same as Z_0, the termination impedance, because the in-phase T-junctions in Fig. 2(a) are turned around. The value of R_0 can be divided into two resistors R_1 and R_2 as shown in Fig. 3(c), and the relation among the three resistance values of R_0, R_1 and R_2 yields

$$\frac{R_1 R_2}{R_1 + R_2} = R_0 = Z_0 \tag{11}$$

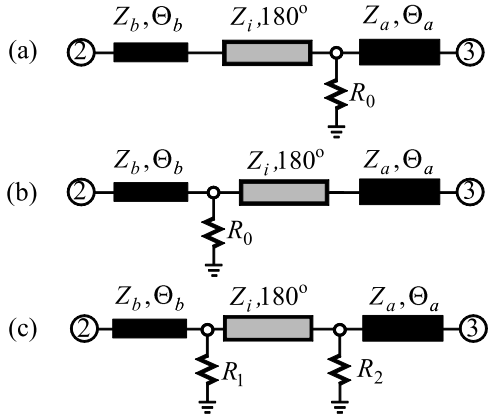

FIGURE 3. Isolation circuits based on the in-phase T-junctions. (a) One isolation resistor between the two TLs with Z_a and Z_i. (b) One isolation resistor between the two TLs with Z_b and Z_i. (c) Two isolation resistors located at both ends of the TL with Z_i.

With $R_0 = Z_0$ in Fig. 3(a) and (b), the third port can be made where the resistance R_0 is connected, leading to a balun T-junction. Therefore the Gysel power divider can be applied not only for the in-phase power divider but also for the out-of-phase power divider (balun).

IV. DESIGN PARAMETERS AND FREQUENCY RESPONSES

Depending on the design formulas of Z_a and Z_b (8), many combinations of Θ_a and Θ_b are available, and two with $\Theta_a + \Theta_b = 90°$ and 95° will be treated by varying the power-division ratios of k^2. The design parameters for $\Theta_a + \Theta_b = 90°$ are listed in Table 2, while those with $\Theta_a + \Theta_b = 95°$ in Table 3 where all the values are in Ω, and the values of Z_b should be greater than those of Z_a due to the assumed $k \geq 1$. The design parameters in both Tables find that the characteristic impedances of Z_a and Z_b are proportional to the power-division ratios, when the sum of $\Theta_a + \Theta_b$ is fixed,

TABLE 2. Design parameters for $Z_0 = Y_0^{-1} = 50$ Ω fixing $\Theta_a + \Theta_b = 90°$.

Θ_a \ k^2		10 dB	12 dB	14 dB	16 dB	18 dB
25 (°)	Z_a	16.1	23.1	28.6	33.0	36.5
	Z_b	23.7	42.8	66.9	97.1	135
35 (°)	Z_a	27.4	32.1	35.8	38.7	41.0
	Z_b	60.7	89.4	125	171	228
40 (°)	Z_a	31.2	35.0	38.1	40.6	42.5
	Z_b	82.7	117	160	214	283
45 (°)	Z_a	34.2	37.4	40.0	42.1	43.7
	Z_b	108	149	200	265	347

TABLE 3. Design parameters for $Z_0 = Y_0^{-1} = 50$ Ω Fixing $\Theta_a + \Theta_b = 95°$.

Θ_a \ k^2		10 dB	12 dB	14 dB	16 dB	18 dB
20 (°)	Z_a	34.7	33.9	34.9	36.8	38.9
	Z_b	38.9	47.7	62.0	82.2	109
30 (°)	Z_a	31.7	34.4	36.9	39.3	41.3
	Z_b	55.4	75.4	102	137	181
40 (°)	Z_a	35.0	37.7	40.0	41.9	43.5
	Z_b	86.8	117	157	207	271
50 (°)	Z_a	38. 6	40.8	42.6	44.0	45.2
	Z_b	132	176	231	301	389

and if the difference between Θ_a and Θ_b is bigger, the values of Z_b become to be lower.

That is, to have feasible characteristic impedance of Z_b, Θ_a should be shorter, and the difference between Θ_a and Θ_b should be bigger, when the desirable power-division ratio and the sum of $\Theta_a + \Theta_b$ are fixed. Under the assumption that the highest feasible characteristic impedance is 160 Ω, the feasible cases are marked in Tables 2 and 3. For the conventional cases in [18] and [24], when $k^2 = 16$ and 18 dB, the values of Z_b should be 319.42 and 400.3 Ω, respectively. However with $\Theta_a = 25°$ in Table 2, $Z_b = 97.1$ and 135 Ω are sufficient for $k^2 = 16$ dB and 18 dB, respectively.

The characteristic impedances of Z_a and Z_b are plotted in Fig. 4 for the cases of $\Theta_a = \Theta_b$, the same as [15]. The plots in Fig. 4 find that the characteristic impedances of Z_b are proportional to the electrical lengths of $\Theta_a = \Theta_b$, and the electrical lengths of $\Theta_a = \Theta_b$ should be less than 73.99° for $k^2 = 10$ dB, when the highest feasible characteristic impedance is assumed to be 160 Ω. For $k^2 = 12$ dB, the values of Z_b are greater than 160 Ω when $\Theta_a = \Theta_b$ is greater than 50° as shown in Fig. 4.

Considering that with $\Theta_a = \Theta_b = 90°$ [18], [24], the value of Z_b should be 165.83 Ω for $k^2 = 10$ dB, arbitrary values of $\Theta_a = \Theta_b$ in Fig. 4 [15] can alleviate somehow the conventional issue of the high impedance TLs but cannot be a fundamental solution to the problem. Therefore it can be concluded that the proposed topology in Fig. 2 has advantage

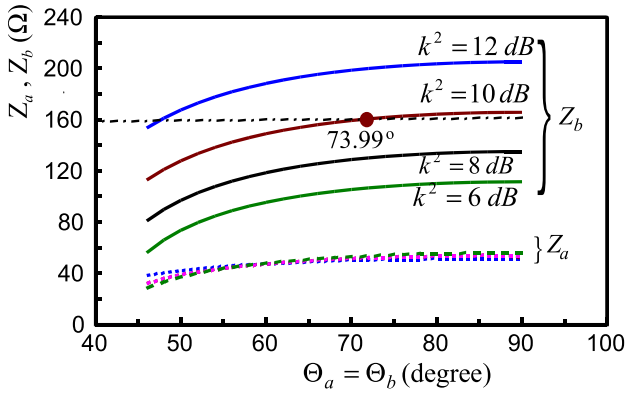

FIGURE 4. The values of Z_a and Z_b with $\Theta_a = \Theta_b$ in [15].

on any conventional in-phase T-junction in terms of high power-division ratios without high impedance TLs.

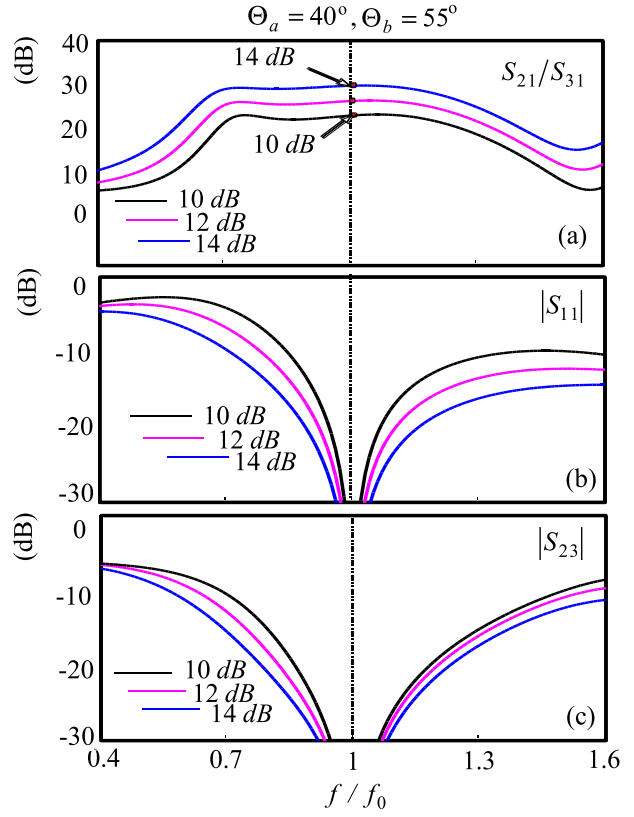

FIGURE 5. Frequency responses of Gysel power dividers with $\Theta_a = 40°$ and $\Theta_b = 55°$. (a) Power-division ratios. (b) $|S_{11}|$ (c) $|S_{23}|$.

The cases for $\Theta_a = 40°$ and $\Theta_b = 55°$ in Table 3 were simulated for $k^2 = 10$, 12 and 14 dB, based on the isolation circuit in Fig. 3(a) with $Z_i = 50\ \Omega$ and $R_0 = 50\ \Omega$. The frequency responses are plotted in Fig. 5 where f_0 and f are design and operating frequencies, respectively. The power-division ratios of S_{21}/S_{31} are in Fig. 5(a), while the frequency responses of $|S_{11}|$ and the isolations of $|S_{23}|$ are in Fig. 5(b) and (c), respectively. If the perfect isolations of $|S_{23}|$ are achieved, the output matching of $|S_{22}|$ and $|S_{33}|$ are guaranteed. Therefore the frequency responses of $|S_{22}|$ and $|S_{33}|$ are not treated. For all cases, designed power-division ratios are achieved at f_0 in Fig. 5(a), port ① is perfectly matched at f_0 in Fig. 5(b), perfect isolation between ports ② and ③ can be achieved at f_0, as well in Fig. 5(c). The frequency responses in Fig. 5 show that with the power-division ratios bigger, the bandwidths of $|S_{11}|$ and $|S_{23}|$ become wider.

V. MEASUREMENTS AND COMPARISONS

For the proof-of-concept demonstration, two prototypes I and II for the power-division ratios of $k^2 = 17$ dB and 20 dB respectively were fabricated on a substrate (RT/duriod 5870, $\varepsilon_r = 2.33$, $H = 62\ mil$) and tested at $f_0 = 1$ GHz.

A. PROTOTYPE I FOR $k^2 = 17$ dB

For $k^2 = 17$ dB, the two electrical lengths of $\Theta_a = 30°$ and $\Theta_b = 70°$ were selected so that the characteristic impedance of Z_b can be feasible, calculating $Z_a = 42.89\ \Omega$ and $Z_b = 161.56\ \Omega$. For the substrate, the width of the TL with Z_a is relatively wide, compared to that with Z_b, and therefore the line width needs to be reduced by using T-type with a stepped-impedance (SI) open stub [26] as shown in Fig. 6(b) where it consists of one TL with Z_p and Θ_p and one SI open stub with two TLs. The characteristic impedance and electrical length of one TL of the SI open stub in Fig. 6(b) are Z_{s1} and Θ_{s1}, while those of another one are Z_{op} and Θ_{op}. The relations between the TL with Z_a and Θ_a and T-type [28] are

$$Z_p = Z_a \frac{\tan\frac{\Theta_a}{2}}{\tan\frac{\Theta_P}{2}} \tag{12a}$$

$$Z_{s1}\frac{Z_{op}\cot\Theta_{op} - Z_{s1}tan\Theta_{s1}}{Z_{s1} + Z_{op}\cot\Theta_{op}\tan\Theta_{s1}} = \frac{Z_p}{2}\frac{Z_p tan\frac{\Theta_P}{2} + Z_a cot\frac{\Theta_a}{2}}{Z_p - Z_a cot\frac{\Theta_a}{2} tan\frac{\Theta_P}{2}} \tag{12b}$$

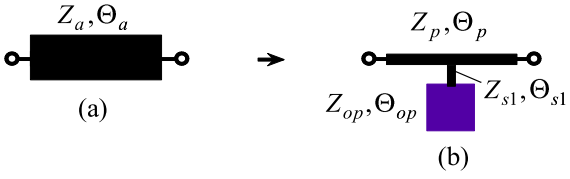

FIGURE 6. Conversion of the TL with Z_a and Θ_a into T-type with a SI open stub. (a) TL with Z_a. (b) T-type with a SI open stub.

When the characteristic impedance of Z_p is fixed at 80 Ω arbitrarily, Θ_p is computed using (12a) as $\Theta_p = 16.35°$. With the known values of Z_a, Θ_a, Z_p and Θ_p, the right term (12b) can be known. If the values of Z_{s1} and Θ_{s1} are selected as $Z_{s1} = 100\ \Omega$ and $\Theta_{s1} = 10°$ arbitrarily along with $Z_{op} = 50\ \Omega$, the electrical length of Θ_{op} can be calculated as $\Theta_{op} = 15.9°$. Even though the TL with Z_a and Θ_a becomes thinner and shorter as desired, the frequency responses of the T-type and the original TL should be about the same, because the TL is very short, referring to [26, Fig. 10]. In this way, all the design parameters are collected in Table 4 where the

TABLE 4. Design and fabrication parameters for prototype I with $k^2 = 17$ dB.

(Z_a, Θ_a)	(Z_b, Θ_b)	IC
(42.89 Ω, 30°)	(161.56 Ω, 70°)	$Z_i = 90\ \Omega$, $R_0 = 50\ \Omega$
$Z_p = 80\ \Omega$, $\Theta_p = 16.35°$, $Z_{s1} = 100\ \Omega$, $\Theta_{s1} = 10°$, $Z_{op} = 50\ \Omega$, $\Theta_{op} = 15.9°$.		
$w_{Z_p} = 2.11$, $\ell_{\Theta_p} = 9.92$, $w_{Z_{s1}} = 1.33$, $\ell_{\Theta_{s1}} = 6.14$, $w_{Z_{op}} = 4.67$, $\ell_{\Theta_{op}} = 9.42$, $w_{Z_b} = 0.34$, $\ell_{\Theta_b} = 43.8$, $w_{Z_i} = 1.67$, $\ell_{\Theta_i} = 111$		

Dimensions in mm.

TABLE 5. Design and fabrication parameters for prototype II with $k^2 = 20$ dB.

(Z_a, Θ_a)	(Z_b, Θ_b)	IC
(52.55 Ω, 18°)	(162.4 Ω, 90°)	$Z_i = 90\ \Omega$, $R_0 = 50\ \Omega$
$Z_p = 70\ \Omega$, $\Theta_p = 13.56°$, $Z_{s1} = 100\ \Omega$, $\Theta_{s1} = 6°$, $Z_{op} = 50\ \Omega$, $\Theta_{op} = 4.22°$.		
$w_{Z_p} = 2.7$, $\ell_{\Theta_p} = 8.2$, $w_{Z_{s1}} = 1.33$, $\ell_{\Theta_{s1}} = 3.68$, $w_{Z_{op}} = 4.67$, $\ell_{\Theta_{op}} = 2.5$, $w_{Z_b} = 0.33$, $\ell_{\Theta_b} = 56.4$, $w_{Z_i} = 1.67$, $\ell_{\Theta_i} = 111$		

Dimensions in mm.

widths and lengths of the TLs are expressed in this way as w_{Z_p} and ℓ_{Θ_p} for the TL with Z_p and Θ_p, respectively, and the line length of the 180° TL with Z_i is written as ℓ_{Θ_i}.

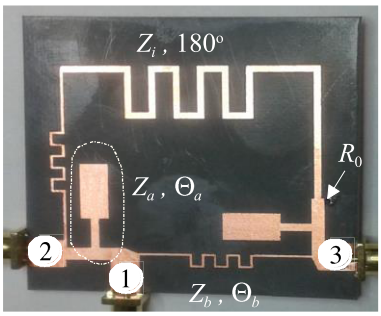

FIGURE 7. Fabricated prototype I for $k^2 = 17$ dB.

The fabricated prototype I for $k^2 = 17$ dB is displayed in Fig. 7 with the isolation circuit in Fig. 3(a). The measured frequency responses of the prototype I are compared with the predicted ones in Fig. 8 where the solid lines are the measured responses, while dotted lines are the predicted ones. The power-division ratio of S_{21}/S_{31} is plotted in Fig. 8(a), while those of matching at all ports and the isolations are in Fig. 8(b) and (c), respectively. At the design frequency of 1 GHz, the measured power-division ratio is 16.68 dB close to 17 dB. The matching values of $|S_{11}|$, $|S_{22}|$ and $|S_{33}|$ are −27.82 dB, −25.96 dB and −20.76 dB, respectively, and the measured isolation is −20.9 dB. As mentioned

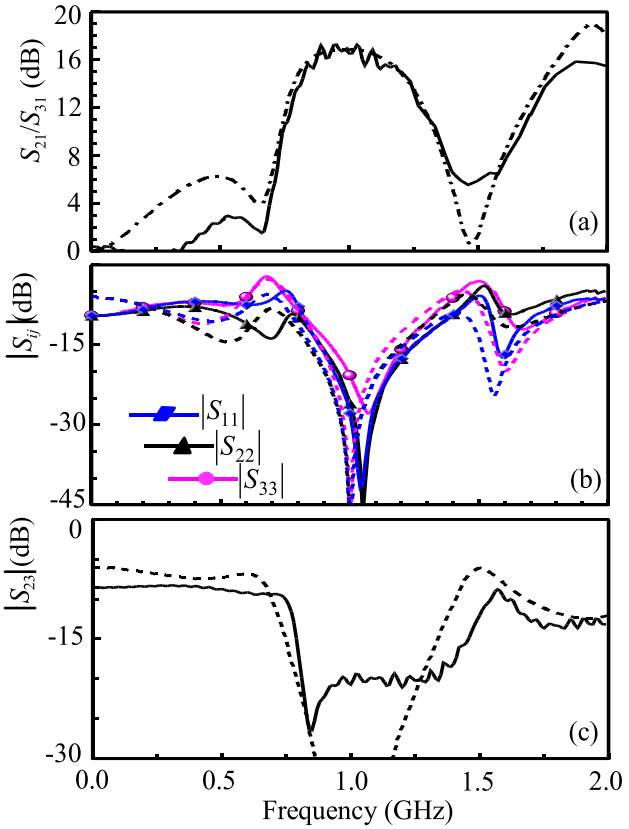

FIGURE 8. Measured (solid lines) and predicted (dotted lines) frequency responses of prototype I. (a) Power-division ratio (S_{21}/S_{31}). (b) Matchings ($|S_{11}|$, $|S_{22}|$, $|S_{33}|$). (c) Isolation ($|S_{23}|$).

regarding (10), the phase difference between the *IC* and the in-phase T-junction should be 180° out of phase. However, the phase differences outside of 1 GHz cannot be the same as those designed, due to fabrication errors which is the reason for the discrepancy between measured and predicted responses in Fig. 8(c). Except that point, the measured responses are in good agreement with the predicted ones.

B. PROTOTYPE II FOR $k^2 = 20$ dB

For $k^2 = 20$ dB, the two electrical lengths of $\Theta_a = 18°$ and $\Theta_b = 90°$ were selected, calculating $Z_a = 52.55\ \Omega$ and $Z_b = 162.4\ \Omega$. In a similar way, the T-type for the TL with Z_a and Θ_a can be designed, and the design parameters are collected in Table 5 where the design parameters of the T-type are $Z_p = 70\ \Omega$, $\Theta_p = 13.56°$, $Z_{s1} = 100\ \Omega$, $\Theta_{s1} = 6°$, $Z_{op} = 50\ \Omega$ and $\Theta_{op} = 4.22°$. The fabricated prototype II is illustrated in Fig. 9 where the isolation circuit is that in Fig. 3(a).

The measured frequency responses of the prototype II are compared with the predicted ones in Fig. 10 where the solid lines are the measured responses, while dotted lines are the predicted ones. The power-division ratio of S_{21}/S_{31} is plotted in Fig. 10(a), while those of matching at all ports and the isolation are in Fig. 10(b) and (c), respectively. At the design frequency of 1 GHz, the measured power-division ratio is 19.75 dB close to 20 dB. The matching values of $|S_{11}|$,

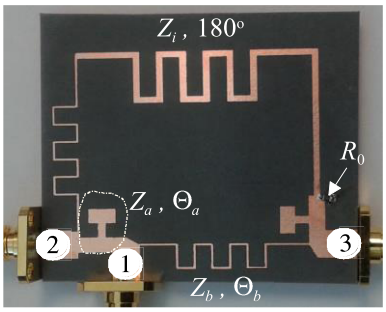

FIGURE 9. Fabricated prototype II for $k^2 = 20$ dB.

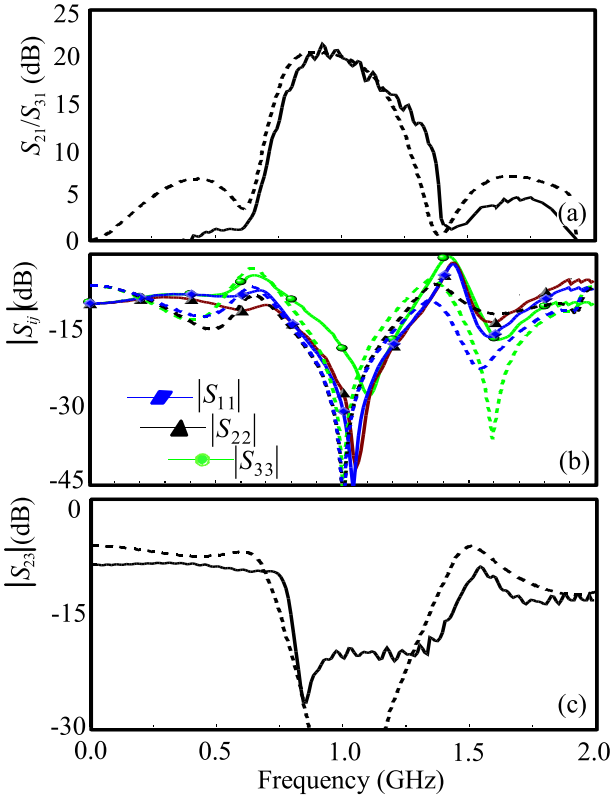

FIGURE 10. Measured (solid lines) and predicted (dotted lines) frequency responses of prototype II. (a) Power-division ratio (S_{21}/S_{31}). (b) Matchings ($|S_{11}|$, $|S_{22}|$, $|S_{33}|$). (c) Isolation ($|S_{23}|$).

$|S_{22}|$ and $|S_{33}|$ are −30.61 dB, −29.95 dB and −18.54 dB, respectively, and the measured isolation is −20.70 dB. The measured responses are in good agreement with the predicted ones, given the fabrication errors.

C. COMPARISONS WITH CONVENTIONAL WORKS

Conventional three- or four-port power dividers consisting of the in-phase T-junctions for the power-division ratios higher than 9 dB are compared to two prototypes I and II, and the comparison results are listed in Table 6 where the power-division ratios are expressed in dB, and power divider types are Gysel power dividers (GPDs), three-port power dividers (TPDs) and ring hybrids (RHs). For all except the proposed prototypes I and II, [4] and [20], high impedance TLs are required as written in Table 6 for such high power-division ratios. Nevertheless, the highest power-division ratio of the conventional works demonstrated so far is 13 dB for the ring hybrid in [17], because it requires the high impedance TLs. On the other hand, the measured prototypes I and II verify that even with such high power-division ratios of 17 dB and 20 dB, the proposed Gysel power dividers can be fabricated without any additional high impedance TLs.

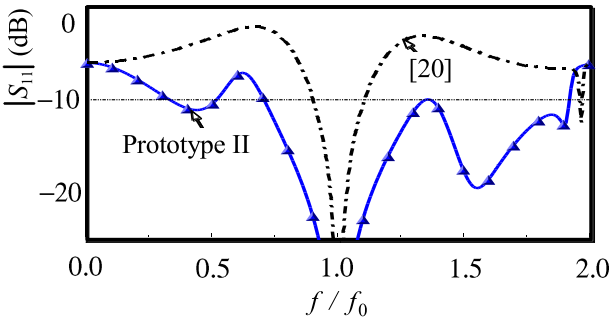

FIGURE 11. Compared frequency responses of the prototype II and [20] for $k^2 = 20$ dB.

TABLE 6. Comparisons with conventional power dividers.

refs.	k^2 (dB)	Types	High Impedance TLs	Fabrication
This work	17 20	GPDs	No	Microstrip
[3]	9.5	TPD	Series inductance	Microstrip
[4]	10	TPD	No	Microstrip
[6]	9.5	TPD	Shunt inductance	Microstrip
[7]	9.5	TPD	Series inductance	Microstrip
[8]	9.5	TPD	Coupled TLs	Microstrip
[10]	10	GPD	Coupled TLs	Microstrip
[14]	10	GPD	Coupled TLs	Microstrip
[16]	12	RH	Series Inductance	Microstrip
[17]	13	RH	Series Inductance	Microstrip
[20]	10	RH	No	Microstrip
[23]	12	RH	Artificial TLs	Microstrip

The power divider in [4] does not need the high impedance TLs but cannot be applied for the Gysel power dividers, while the one in [20] can be used for the Gysel power divider. The prototype II for $k^2 = 20$ dB is compared to that in [20], and the compared frequency responses of $|S_{11}|$ are plotted in Fig. 11. The design parameters for [20] are $Z_a = Z_b = 50\ \Omega$, $\Theta_a = 5.73°$ and $\Theta_b = 87.13°$ in Fig. 1. The 10-dB return loss bandwidth of the prototype II in Fig. 11 is 0.71 −1.92 f_0, 120 %, while that for [20] is 0.9-1.1 f_0, 20 %. Considering all aspects, the suggested Gysel power dividers have definite advantages on the conventional works for high power-division ratios for wider bandwidths.

VI. CONCLUSIONS

In this paper, a novel topology of Gysel power divider was proposed for high power-division ratios, which can be

fabricated without any high impedance TLs even for the power-division ratio of 20 dB. For the design formulas, a study on the in-phase T-junctions of the conventional Gysel/Wilkinson power dividers and ring hybrids was carried out, and two important conditions were newly derived for the arbitrary power-division ratios and perfect matching at all ports. Based on the derived new conditions, the isolation circuits could be derived easily without any additional effort, regardless of symmetric or asymmetric in-phase T-junctions.

For the proof-of-concept demonstration, two prototypes I and II of the Gysel power dividers were fabricated without any high impedance TL for the power-division ratios of 17 dB and 20 dB, respectively, which have never been tried before, and compared with more than ten conventional works with the power-division ratios higher than 9.5 dB. For the further demonstration of the advantage of the suggested work, the frequency response of the prototype II was compared to that [20] requiring no high impedance TL, verifying that the 10-dB return loss bandwidth of the prototype II was about six times wider than that of [20].

Considering all aspects in terms of easy fabrication and bandwidths for high power-division ratios, it can be concluded that the proposed Gysel power dividers have definite advantages on the conventional works and can be implemented for the diverse applications.

REFERENCES

[1] E. J. Wilkinson, "An N-way hybrid power divider," *IRE Trans. Microw. Theory Techn.*, vol. 8, no. 1, pp. 116–118, Jan. 1960.

[2] H.-R. Ahn, "Modified asymmetric impedance transformers (MCCTs and MCVTs) and their application to impedance-transforming three-port 3-dB power dividers," *IEEE Trans. Microw. Theory Techn.*, vol. 59, no. 12, pp. 3312–3321, Dec. 2011.

[3] H.-R. Ahn, "Compact CVT-/CCT-Unequal power dividers for high-power division ratios and design methods for arbitrary phase differences," *IEEE Trans. Microw. Theory Techn.*, vol. 62, no. 12, pp. 2954–2964, Dec. 2014.

[4] H.-R. Ahn, Y. Kim, and B. Kim, "Planar 10:1 unequal three-port power dividers using general design equations," *Electron. Lett.*, vol. 48, no. 15, pp. 934–935, Jul. 2012.

[5] K.-K. M. Cheng and P.-W. Li, "A novel power-divider design with unequal power-dividing ratio and simple layout," *IEEE Trans. Microw. Theory Techn.*, vol. 57, no. 6, pp. 1589–1594, Jun. 2009.

[6] J. L. Li and B. Z. Wang, "Novel design of Wilkinson power dividers with arbitrary power division ratios," *IEEE Trans. Ind. Electron.*, vol. 58, no. 6, pp. 2541–2546, Jun. 2011.

[7] R. Mirzavand, M. M. Honari, A. Abdipour, and G. Moradi, "Compact microstrip Wilkinson power dividers with harmonic suppression and arbitrary power division ratios," *IEEE Trans. Microw. Theory Techn.*, vol. 61, no. 1, pp. 61–68, Jan. 2013.

[8] B. Li, X. Wu, and W. Wu, "A 10:1 unequal wilkinson power divider using coupled lines with two shorts," *IEEE Microw. Wireless Compon. Lett.*, vol. 19, no. 12, pp. 789–791, Dec. 2009.

[9] H.-R. Ahn and B. Kim, "Toward integrated circuit size reduction," *IEEE Microw. Mag.*, vol. 9, no. 1, pp. 65–75, Feb. 2008.

[10] K.-X. Wang, X. Y. Zhang, and B.-J. Hu, "Gysel power divider with arbitrary power ratios and filtering responses using coupling structure," *IEEE Trans. Microw. Theory Techn.*, vol. 62, no. 3, pp. 431–440, Mar. 2014.

[11] X. Wang, K.-L. Wu, and W.-Y. Yin, "A compact Gysel power divider with unequal power-dividing ratio using one resistor," *IEEE Trans. Microw. Theory Techn.*, vol. 62, no. 7, pp. 1480–1486, Jul. 2014.

[12] Z. Sun, L. Zhang, Y. Liu, and X. Tong, "Modified Gysel power divider for dual-band applications," *IEEE Microw. Wireless Compon. Lett.*, vol. 21, no. 1, pp. 16–18, Jan. 2011.

[13] A. M. Abbosh, "Planar out-of-phase power divider/combiner for wideband high power microwave applications," *IEEE Trans. Compon., Packag., Manuf. Technol.*, vol. 4, no. 3, pp. 465–471, Mar. 2014.

[14] S. Chen, Y. Yu, and M. Tang, "Planar out-of-phase Gysel power divider with high power splitting ratio," *Electron. Lett.*, vol. 51, no. 24, pp. 2010–2012, Nov. 2015.

[15] F. Lin, Q.-X. Chu, Z. Gong, and Z. Lin, "Compact broadband Gysel power divider with arbitrary power-dividing ratio using microstrip/slotline phase inverter," *IEEE Trans. Microw. Theory Techn.*, vol. 60, no. 5, pp. 1226–1234, May 2012.

[16] H.-R. Ahn and M. M. Tentzeris, "A novel wideband compact microstrip coupled-line ring hybrid for arbitrarily high power-division ratios," *IEEE Trans. Circuits Syst., II, Exp. Briefs*, vol. 64, no. 6, pp. 630–634, Jun. 2017.

[17] H.-R. Ahn and S. Nam, "Wideband microstrip coupled-line ring hybrids for high power-division ratios," *IEEE Trans. Microw. Theory Techn.*, vol. 61, no. 5, pp. 1768–1780, May 2013.

[18] C. Y. Pon, "Hybrid-ring directional coupler for arbitrary power divisions," *IRE Trans. Microw. Theory Techn.*, vol. 9, no. 6, pp. 529–535, Nov. 1961.

[19] B.-H. Murgulescu, E. Moisan, P. Legaud, E. Penard, and I. Zaquine, "New wideband, $0.67\lambda_g$ circumference 180° hybrid ring coupler," *Electron. Lett.*, vol. 30, no. 4, pp. 299–300, Feb. 1994.

[20] M.-J. Park and B. Lee, "Design of ring couplers for arbitrary power division with 50Ω Lines," *IEEE Microw. Wireless Compon. Lett.*, vol. 21, no. 4, pp. 185–187, Apr. 2011.

[21] L.-S. Wu, J. Mao, and W.-Y. Yin, "Miniaturization of rat-race coupler with dual-band arbitrary power divisions based on stepped-impedance double-sided parallel-strip line," *IEEE Trans. Compon., Packag., Manuf. Technol.*, vol. 2, no. 12, pp. 2017–2030, Dec. 2012.

[22] M.-J. Park and B. Lee, "A universal ring 0°/180° coupler for arbitrary power division," *Microw. Opt. Technol. Lett.*, vol. 55, no. 3, pp. 543–547, Mar. 2013.

[23] K.-L. Ho and P.-L. Chi, "Miniaturized and large-division-ratio ring coupler using novel transmission-line elements," *IEEE Microw. Wireless Compon. Lett.*, vol. 24, no. 1, pp. 35–37, Jan. 2014.

[24] H.-R. Ahn, I. Wolff, and I.-S. Chang, "Arbitrary termination impedances, arbitrary power divisions and small-sized ring hybrids," *IEEE Trans. Microw. Theory Techn.*, vol. 45, no. 12, pp. 2241–2247, Dec. 1997.

[25] H.-R. Ahn, "Comments on 'Converting baluns into broad-band impedance-transforming 180° hybrids,'" *IEEE Trans. Microw. Theory Tech.*, vol. 52, no. 1, pp. 228–230, Dec. 2004.

[26] H.-R. Ahn and S. Nam, "Compact microstrip 3-dB coupled-line ring and branch-line hybrids with new symmetric equivalent circuits," *IEEE Trans. Microw. Theory Techn.*, vol. 61, no. 3, pp. 1067–1078, Mar. 2013.

[27] H.-R. Ahn, *Asymmetric Passive Components in Microwave Integrated Circuits*. New York, NY, USA: Wiley, 2006.

[28] H.-R. Ahn and S. Nam, "New design formulas for impedance-transforming 3-dB marchand baluns," *IEEE Trans. Microw. Theory Techn.*, vol. 59, no. 11, pp. 2816–2823, Nov. 2011.

HEE-RAN AHN (S'90–M'95–SM'99) received the B.S., M.S., and Ph.D. degrees in electronic engineering from Sogang University, Seoul, South Korea.

From 1996 to 2002, she was with the Department of Electrical Engineering, Duisburg-Essen University, Duisburg, Germany, where she was involved in the Habilitation dealing with asymmetric passive components in microwave integrated circuits. From 2003 to 2005, she was with the Department of Electrical Engineering and Computer Science, Korea Advanced Institute of Science and Technology, Daejeon, South Korea. From 2005 to 2009, she was with the Department of Electronics and Electrical Engineering, Pohang University of Science and Technology, Pohang, South Korea. From 2009 to 2010, she was with the Department of Electrical Engineering, University of California at Los Angeles, Los Angeles, CA, USA. From 2011 to 2014, she was with the School of Electrical Engineering and Computer Science, Seoul National University, Seoul. Since 2015, she has been with the School of Electrical and Computer Engineering, Georgia Institute of Technology, Atlanta, GA, USA, as a Visiting Scholar. She has authored the book entitled *Asymmetric Passive Component in Microwave Integrated Circuits* (Wiley, 2006). Her current research interests include high-frequency and microwave circuit designs and biomedical applications using microwave theory and techniques.

MANOS M. TENTZERIS received the Diploma degree *(magna cum laude)* in electrical and computer engineering from the National Technical University of Athens, Greece, and the M.S. and Ph.D. degrees in electrical engineering and computer science from The University of Michigan, Ann Arbor, MI, USA. He was a Visiting Professor with the Technical University of Munich, Germany, in 2002, GTRI-Ireland, Athlone, Ireland, in 2009, and LAAS-CNRS, Toulouse, France, in 2010. He has served as the Head of the GT-ECE Electromagnetics Technical Interest Group, as the Georgia Electronic Design Center Associate Director for RFID/Sensors Research, as the Georgia Tech NSF-Packaging Research Center Associate Director for RF Research, and as the RF Alliance Leader. He is currently the Ken Byers Professor in flexible electronics with the School of ECE, Georgia Institute of Technology, Atlanta, GA, USA. He also heads the ATHENA Research Group (20 researchers). He has helped to develop academic programs in 3D/inkjet-printed RF electronics and modules, flexible electronics, origami and morphing electromagnetics, highly integrated/multilayer packaging for RF, wireless applications using ceramic and organic flexible materials, paper-based RFIDs and sensors, wireless sensors and biosensors, wearable electronics, green electronics, energy harvesting and wireless power transfer, nanotechnology applications in RF, microwave MEMS, and SOP-integrated (UWB, multiband, mmW, and conformal) antennas. He has authored over 700 papers in refereed journals and conference proceedings, five books, and 25 book chapters. He is a Fellow of the IEEE and the Electromagnetic Academy, a member of the URSI-Commission D, the MTT-15 Committee, and the Technical Chamber of Greece, and an Associate Member of EuMA. He was a recipient/co-recipient of the 1997 Best Paper Award and the 2000 NSF CAREER Award of the International Hybrid Microelectronics and Packaging Society, the 2001 ACES Conference Best Paper Award, the 2002 International Conference on Microwave and Millimeter-Wave Technology Best Paper Award at Beijing, China, the 2002 Georgia Tech-ECE Outstanding Junior Faculty Award, the 2003 NASA Godfrey Art Anzic Collaborative Distinguished Publication Award, the 2003 IBC International Educator of the Year Award, the 2003 IEEE CPMT Outstanding Young Engineer Award, the 2004 IEEE TRANSACTIONS ON ADVANCED PACKAGING Commendable Paper Award, the 2006 IEEE MTT Outstanding Young Engineer Award, the 2006 Asian–Pacific Microwave Conference Award, the 2007 IEEE APS Symposium Best Student Paper Award, the 2007 IEEE IMS Third Best Student Paper Award, the 2007 ISAP 2007 Poster Presentation Award, the 2009 IEEE TRANSACTIONS ON COMPONENTS AND PACKAGING TECHNOLOGIES Best Paper Award, the 2009 E. T. S. Walton Award from the Irish Science Foundation, the 2010 Georgia Tech Senior Faculty Outstanding Undergraduate Research Mentor Award, the 2010 IEEE Antennas and Propagation Society Piergiorgio L. E. Uslenghi Letters Prize Paper Award, the 2011 International Workshop on Structural Health Monitoring Best Student Paper Award, the 2012 FiDiPro Award in Finland, the iCMG Architecture Award of Excellence, the 2013 *IET Microwaves, Antennas and Propagation* Premium Award, the 2014 Georgia Tech ECE Distinguished Faculty Achievement Award, the 2014 IEEE RFID-TA Best Student Paper Award, the 2015 *IET Microwaves, Antennas and Propagation* Premium Award. He was the Chair of the 2005 IEEE CEM-TD Workshop and the TPC Chair of the IEEE IMS 2008 Symposium. He is the Vice-Chair of the RF Technical Committee of the IEEE CPMT Society. He is the Founder and the Chair of the RFID Technical Committee of the IEEE MTT Society and the Secretary/Treasurer of the IEEE C-RFID. He is an Associate Editor of the IEEE TRANSACTIONS ON MICROWAVE THEORY AND TECHNIQUES, the IEEE TRANSACTIONS ON ADVANCED PACKAGING, and the *International Journal on Antennas and Propagation*. He has given more than 100 invited talks to various universities and companies all over the world. He served as one of the IEEE MTT-S Distinguished Microwave Lecturers, from 2010 to 2012, and he is one of the IEEE CRFID Distinguished Lecturers.